A Surface Panel Method for Ducted Propellers with New Wake Model Based on Velocity Measurements

by Chiharu Kawakita*, *Member*

Summary

The velocity distribution downstream of a ducted propeller was measured in a cavitation tunnel by the use of a 3-component Laser Doppler Velocimeter. A considerable amount of change of the hydrodynamic pitch of the ducted propeller was observed in comparison with that of the impeller without duct. Based on these velocity measurements around the ducted propeller, a new wake model considering the effect of impeller loading was proposed to improve the prediction of the hydrodynamic performance for ducted propellers by the surface panel method. The flow fields around the ducted propeller calculated by the use of this method were shown in good agreement with the measured data as expected. The open-water characteristics of ducted propellers calculated by this method also showed good agreement with the experimental data.

1. Introduction

Ducted propellers have been used for ship and underwater vehicle propulsion. The merits of ducted propellers are both to increase propulsive efficiency at heavily loaded condition and to protect the impeller from damage.

Analysis methods for ducted propellers have been developed by many researchers. Surface panel method is one of the most advanced methods for the prediction of the performance for ducted propellers, because it allows precise representations of the complicated geometry. In the surface panel method, hydrodynamic modeling of the trailing vortex wake behind the ducted propeller is one of the most important factors for improving the ducted propeller theories. Recently, the present author[1] has developed a surface panel method in which the flow on the impeller and duct is analyzed simultaneously. He also pointed out the importance of the wake model behind ducted propeller for the accuracy of the calculation.

In the past, Hoshino[2] constructed the realistic wake model for conventional propeller based on the flow field measurements around propellers by Laser Doppler Velocimeter (LDV). In the case of ducted propeller, there are some examples for the velocity measurements by LDV[3),4)]. However, the construction of the realistic wake model for the ducted propeller would not have been done yet.

In the present study, therefore, downstream of a ducted propeller and an impeller without duct are precisely measured for the construction of useful wake model. The measurements were done in a uniform flow in a cavitation tunnel by the use of a 3-component LDV. Three components of the velocities fluctuating periodically at various radii and axial positions downstream of the ducted propeller comparing with those of the impeller without duct are presented. The variation of the hydrodynamic pitch of the ducted propeller is clarified by comparison with that of the impeller without duct.

Based on the measured velocity distribution of the trailing vortex wake of the ducted propeller, a new wake model with considering the effect of impeller loading is proposed. Then flow fields around the ducted propeller were calculated by the use of the surface panel method with this wake model and compared with the measured data. And the applicability of the present method is also investigated by comparing with experimental data for two kinds of ducted propellers.

2. Velocity Measurements Downstream of a Ducted Propeller

2.1 Definitions of Coordinate Systems and Flow Velocities

We consider a ducted propeller rotating clockwise with a constant angular velocity Ω in an inviscid, incompressible, irrotational flow with a uniform axial speed V_A far upstream. The ducted propeller consists of an impeller and an axisymmetric duct set around it. The impeller consists of a finite number of axisymmetrically arranged blades of identical shape and a hub.

* Nagasaki Experimental Tank, Mitsubishi Heavy Industries, Ltd.
Received 9th July 1992
Read at the Autumn meeting 9, 10th Nov. 1992

We define a Cartesian coordinate system O-xyz with origin O fixed at the center of the ducted propeller, where x directs downstream of the ducted propeller as shown in Fig. 1. The z-axis points upward and the y-axis completes a right-handed coordinate system. A cylindrical coordinate system O-$xr\theta$ is also introduced, where θ is angular coordinate and r is radial coordinate. The velocity components in the x-, y-, z-axis directions are denoted by v_x, v_y, v_z, respectively, and the velocity components in the r- and θ-directions by v_r, v_θ.

2.2 Ducted Propeller Model and Conditions of Velocity Measurements

Velocity measurements downstream of a ducted propeller by LDV[5] were carried out in a uniform flow in the cavitation tunnel at Nagasaki Experimental Tank. The ducted propeller model is a five bladed Kaplan type impeller in a combination with NSMB's (now MARIN) nozzle no. 19A. Principal particulars of the ducted propeller model is shown in Table 1. For investigating the effect of duct on the slipstream of impeller, velocity measurements of the impeller without duct also carried out.

In the LDV measurement, rotational speed of impeller n was kept constant at $n=25$ rps and advance speed of the ducted propeller V_A was changed to vary the advance ratio as

$$J=V_A/nD, \tag{2.1}$$

where D is the diameter of impeller. Measurements were done in the following conditions as

$J=0.2, 0.5, 0.8,$ for ducted propeller,

$J=0.5, 0.8,$ for impeller without duct.

The location of the velocity measurements downstream of the ducted propeller by LDV are shown in Fig. 2,

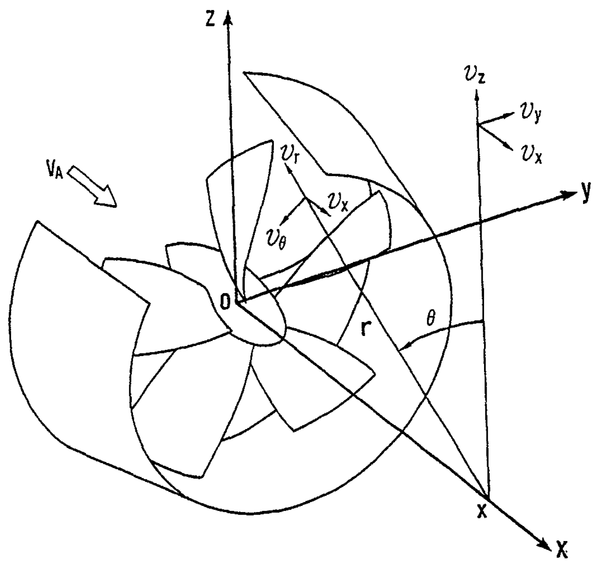

Fig. 1 Coordinate systems of ducted propeller

Table 1 Principal particulars of ducted propeller model

Diameter of Propeller (mm)	221.35
Pitch Ratio	0.9741
Expanded Area Ratio	0.6268
Boss Ratio	0.1882
Number of Blades	5
Rake Angle (deg.)	0.0
Duct Length - Diameter Ratio	0.498
Tip Clearance - Diameter Ratio	0.0072

NSMB Nozzle No.19A

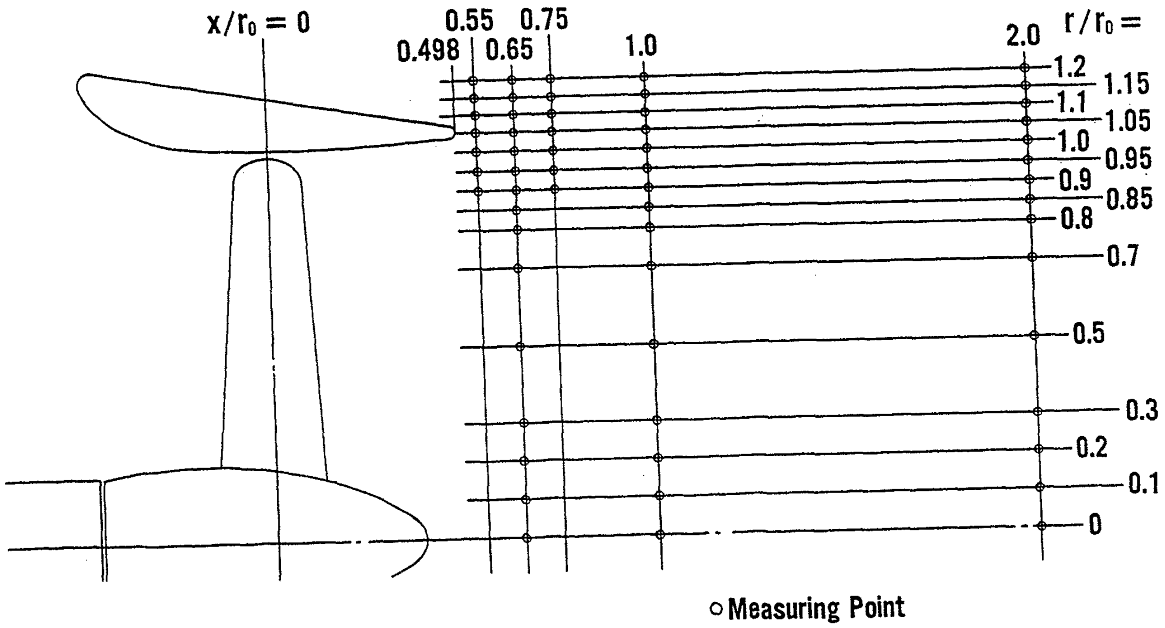

Fig. 2 Location of velocity measurements behind ducted propeller

where r_0 is the radius of impeller.

2.3 Results of Velocity Measurements Downstream of Ducted Propeller

As an example of the results of the LDV measurements, circumferential variations of three components of the velocities downstream of both the ducted propeller and the impeller without duct at the advance ratio of $J=0.50$ and at axial position of $x/r_0=0.65$ just behind the duct are shown in Fig. 3. It is shown that each velocity component is periodically fluctuating with the blade frequency. In both cases, the remarkable change of the radial velocity component shows the velocity jump across the trailing vortex sheet. The slope of the velocity jump of the radial component at inner radii ($r/r_0\leq 0.5$) is opposite to that at outer radii ($r/r_0\geq 0.8$). This shows that the strength of the trailing vortex changes its sign between the inner and outer radii. Further, this corresponds to the opposite slope of the radial circulation distribution at inner and outer radii. The velocity defects in the axial and tangential velocity components observed at the position where the velocity jump of radial component occurred correspond to the viscous wake of the boundary layer on the impeller blades. In the case of the impeller without duct, the great variations of the radial velocity component at $r/r_0=0.90$ seem to be due to strong tip vortices. Therefore, the tip vortices are considered to be located near this radius. On the other hand, in the case of the ducted propeller, the variations of the radial velocity component at $r/r_0=1.00$ due to tip vortices are smaller than

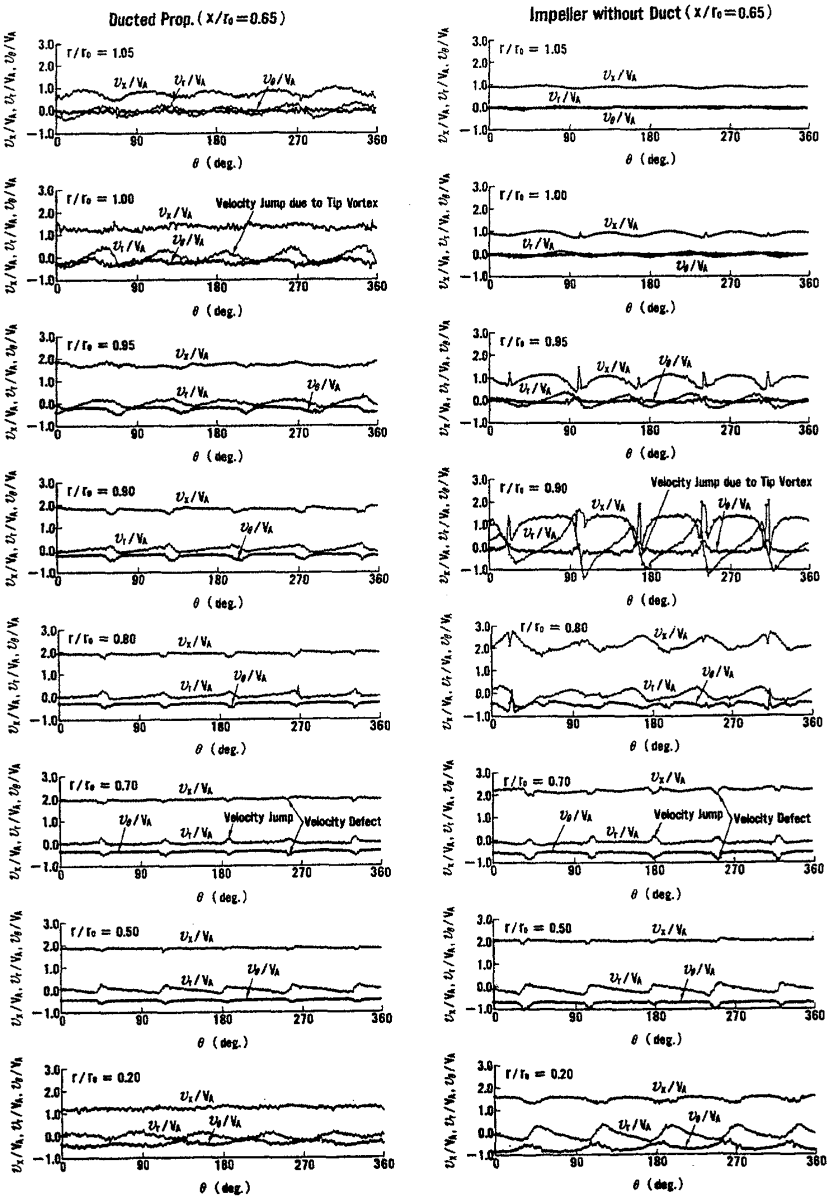

Fig. 3 Circumferential variations of velocities downstream of ducted propeller and impeller without duct ($J=0.50$, $x/r_0=0.65$)

that of the impeller without duct. It shows that the strength of the tip vortices of the impeller of the ducted propeller is weaker than that of the impeller without duct. It is considered that the reason would be that the circulation of the impeller of the ducted propeller decreases for the effect of duct which produces the positive circulation by itself. The axial velocity component of the ducted propeller at $r/r_0=1.05$ is smaller than that of the impeller without duct due to the viscous wake of the boundary layer on the duct.

Velocity distributions downstream (axial positions of $x/r_0=0.65, 1.00, 2.00$) of the ducted propeller at the advance ratio of $J=0.50$ are shown in Figs. 4-6 as the form of the equi-velocity contour curves of axial component and the velocity vectors of cross components in a plane parallel to the propeller plane. Fig. 7 shows an example of the impeller without duct at axial position of $x/r_0=0.65$ and at the advance ratio of $J=0.50$. These

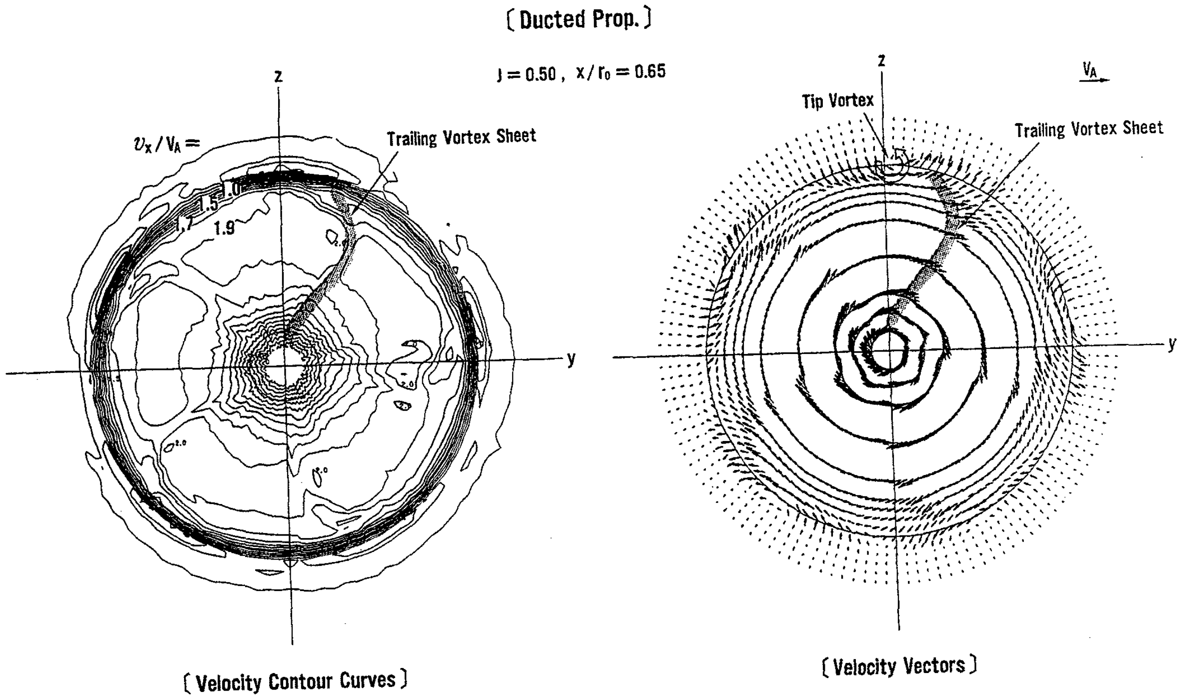

Fig. 4 Velocity distributions downstream of ducted propeller ($J=0.50$, $x/r_0=0.65$)

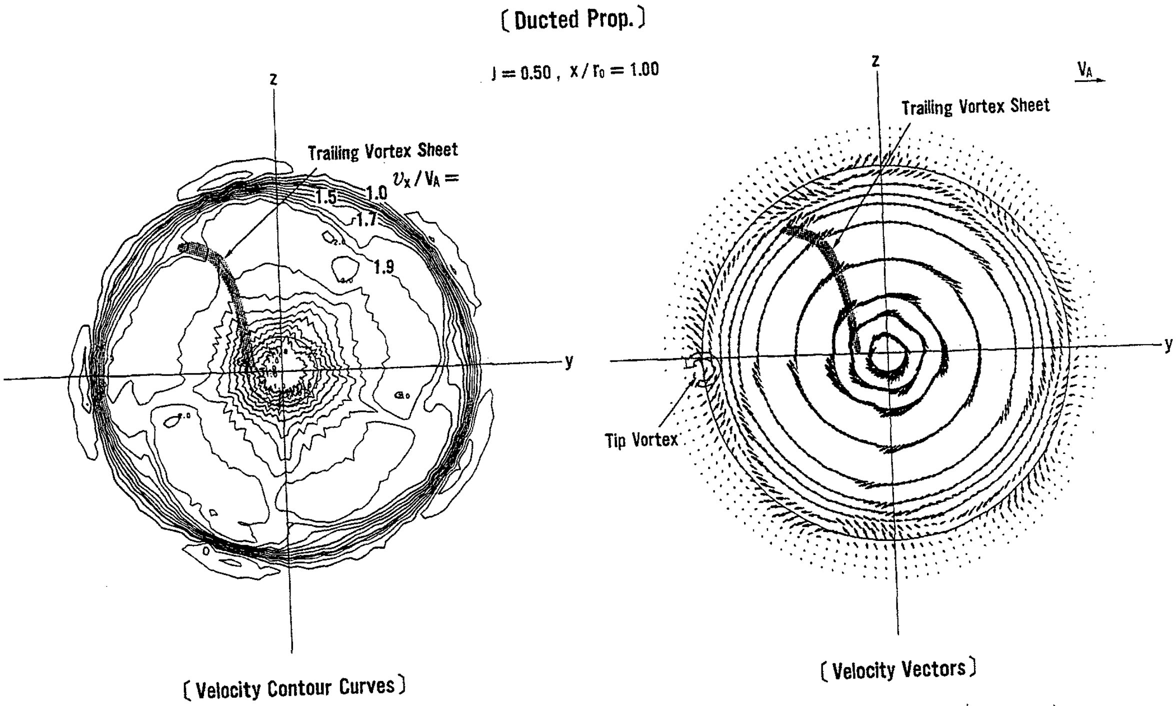

Fig. 5 Velocity distributions downstream of ducted propeller ($J=0.50$, $x/r_0=1.00$)

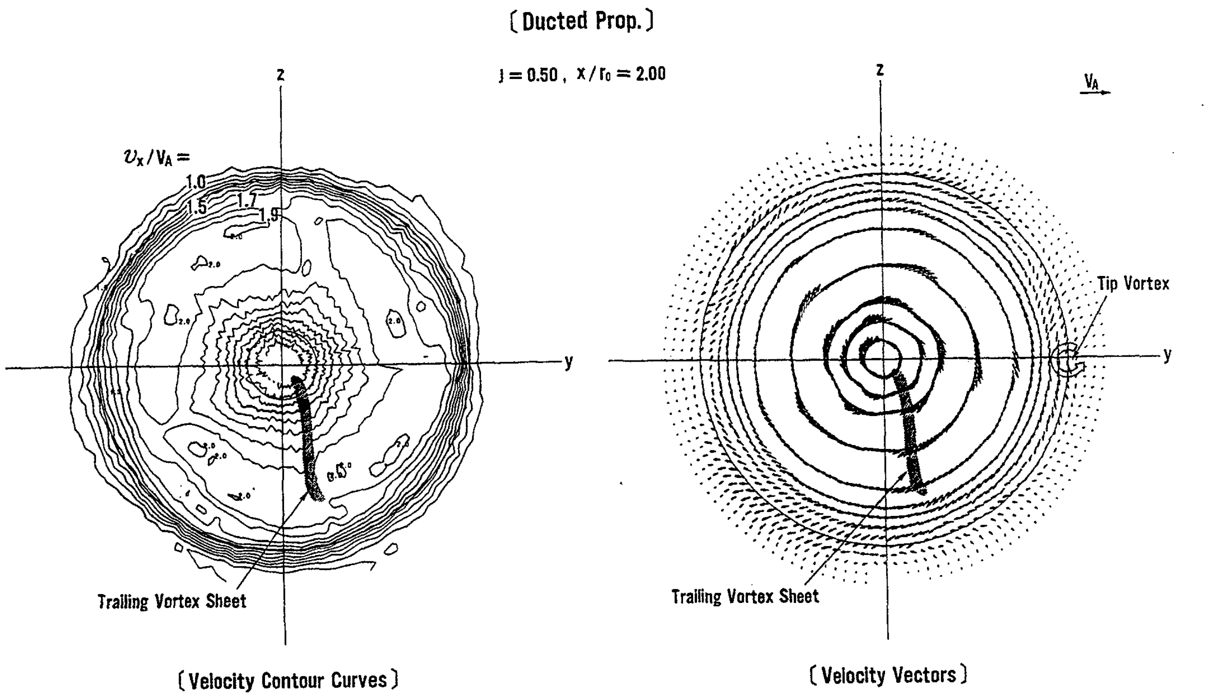

Fig. 6 Velocity distributions downstream of ducted propeller ($J=0.50$, $x/r_0=2.00$)

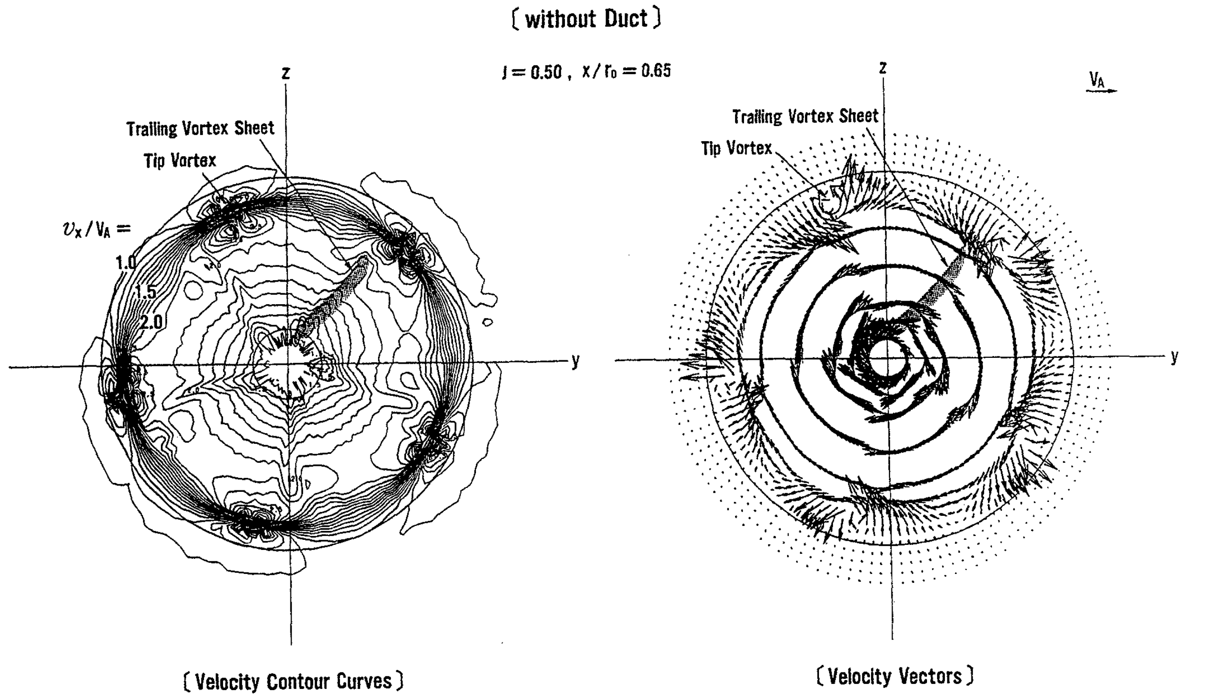

Fig. 7 Velocity distributions downstream of impeller without duct ($J=0.50$, $x/r_0=0.65$)

figures are observed from the downstream side of the ducted propeller and the impeller without duct. In both cases, since the impeller is right-handed, the tip vortices are rotating in the counterclockwise direction as seen in Figs. 4-7. Trailing vortex sheets are observed in these figures. Angular position of tip vortex is larger than that of the trailing vortex sheet and the difference of the angular position is increasing along the downstream direction. This means that the pitch of the tip vortex is smaller than that of the trailing vortex sheet. In the case of the ducted propeller, radial position of the center of the tip vortices is almost constant at the blade tip along the downstream direction. But in the case of the impleller without duct, radial position of the center of the tip vortices moves from the blade tip to the inner radii along the downstream direction. This means that the trailing vortex wake of the impeller without duct brings about the large contraction but that of the ducted propeller brings about the small contraction. Comparing between Fig. 4 and Fig. 7, it is clear that the strength of the tip vorteces of the impeller without duct is considerably stronger than that of the ducted propeller.

2.4 Hydrodynamic Pitch

Using the circumferentially averaged axial and tangential velocities $\bar{v}_x$, $\bar{v}_\theta$, hydrodynamic pitch angle of the trailing vortex wake of the ducted propeller can be calculated by

$$\beta_w=\tan^{-1}\left(\frac{\bar{v}_x}{r\Omega+\bar{v}_\theta}\right). \tag{2.2}$$

An example of radial distributions of the hydrodynamic pitch angles at axial position of $x/r_0=0.65$ just behind the ducted propeller is shown in Fig. 8, comparing with the hydrodynamic pitch angles of the impeller without duct and the geometrical pitch angle defined as follows:

$$\beta_G=\tan^{-1}\left(\frac{P(r)}{2\pi r}\right), \tag{2.3}$$

where $P(r)$ is the geometrical pitch distribution. As the advance ratio increases, the hydrodynamic pitch angle also increases in both cases.

The hydrodynamic pitch P_w of the trailing vortex wake of the ducted propeller can be obtained by

$$P_w(r)=2\pi r\cdot\tan\beta_w. \tag{2.4}$$

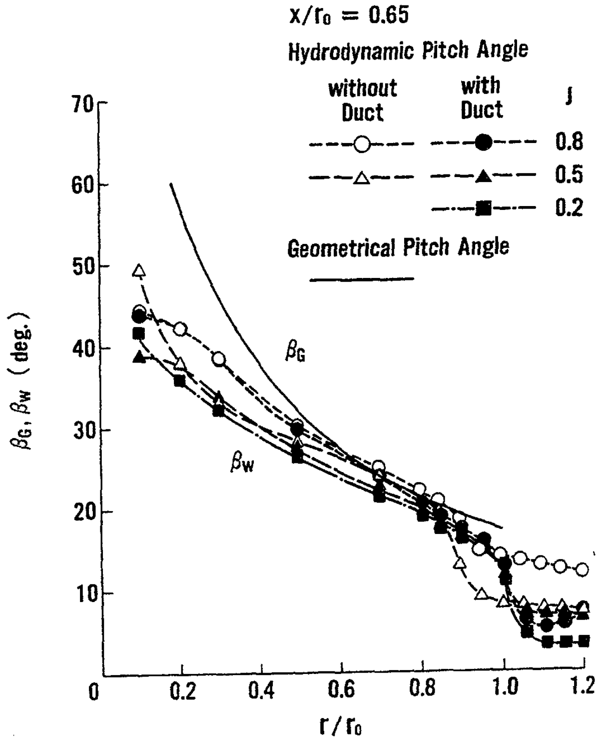

Fig. 8 Comparison of radial distributions of hydrodynamic pitch angle of trailing vortex wake ($x/r_0=0.65$)

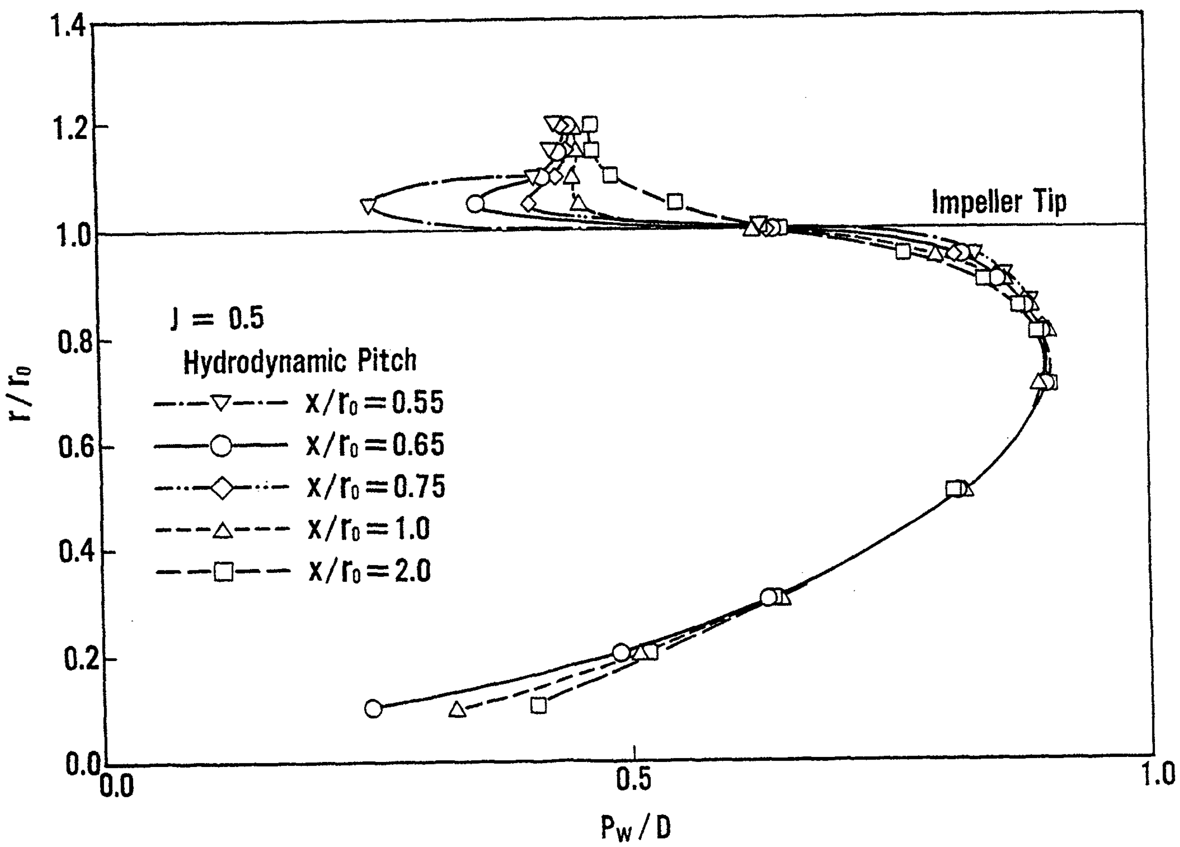

Fig. 9 Variations of hydrodynamic pitch of trailing vortex wake of ducted propeller ($J=0.5$)

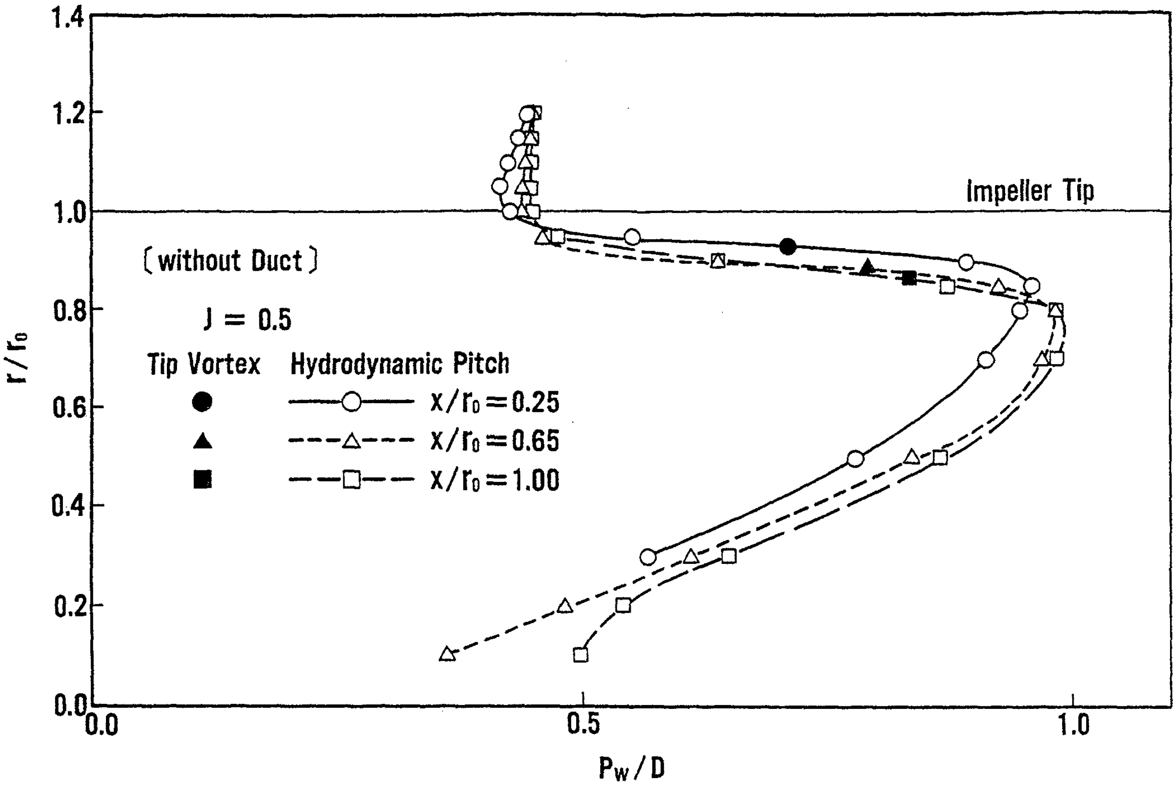

Fig. 10 Variations of hydrodynamic pitch of trailing vortex wake of impeller without duct ($J=0.5$)

Radial distributions of the hydrodynamic pitch downstream of the ducted propeller at the advance ratio of $J=0.50$ are shown in Fig. 9, and those of the impeller without duct are shown in Fig. 10. In the case of the ducted propeller, the hydrodynamic pitch is nearly constant in spite of increase of the distance from the ducted propeller. The constant hydrodynamic pitch of the ducted propeller would be due to the small contraction. On the other hand, the hydrodynamic pitch of the impeller without duct increases as the distance from the impeller increases. Increase in the hydrodynamic pitch of the impeller without duct would be due to the contraction of the trailing vortex wake along the downstream direction. Pitch of the tip vortices is obtained from the axial variations of the angular positions of the center of the tip vortices. That of the impeller without duct increases as the distance from the impeller increases the same as the hydrodynamic pitch. The hydrodynamic pitches of the ducted propeller at various advance ratios are shown in Figs. 11 and 12, comparing with those of the impeller without duct. In both cases, the hydrodynamic pitch becomes large as the advance ratio increases. The hydrodynamic pitch of impeller without duct in the vicinity of the radial position $r/r_0=0.70$ is especially larger than that of the ducted propeller. This means that the effect of the contraction appears in the increase of the hydrodynamic pitch downstream in the vicinity of the impeller tip particularly.

3. Numerical Procedure

3.1 Numerical Modeling of Trailing Vortex Wake

Based on the measured velocity distribution downstream of the ducted propeller, a new wake model which consists of the helical trailing vortex sheet of impeller and the cylindrical trailing vortex sheet of duct is considered. In this study, the trailing vortex wake is divided into two parts, transition wake region and ultimate wake region as shown in Fig. 13. The contraction and the variation of hydrodynamic pitch of the helical trailing vortex sheet of the impeller are considered in the transition wake region. On the other hand, radial positions and pitch of the helical trailing vortex sheet are kept constant in the ultimate wake region. The cylindrical vortex sheet of the duct proceeds downstream in parallel with the contraction of tip vortex from the duct trailing edge. Further, we also construct a wake model of the Kaplan type impeller without duct for investigating the effect of duct.

The contraction of the helical trailing vortex sheet of the ducted propeller and the impeller without duct is considered first. The radial distance from the hub vortex radius $r=r_{wh}$ to the tip vortex radius $r=r_{wT}$ in the ultimate wake is divided into N_R small panel strips. Then the radii of each panel strips can be expressed as follows:

$$r_{w\mu}=\frac{1}{2}(r_{wT}+r_{wh})-\frac{1}{2}(r_{wT}-r_{wh})\cos\alpha_\mu, \qquad (3.1)$$

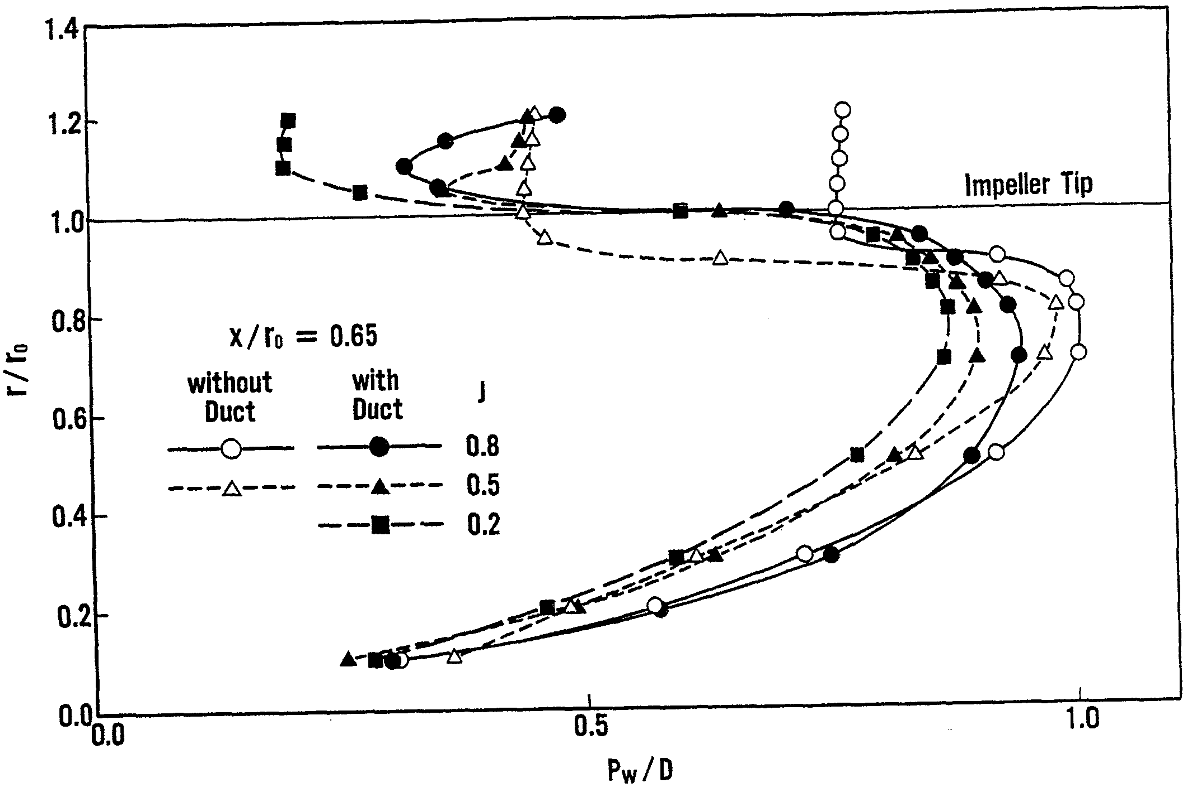

Fig. 11 Comparison of hydrodynamic pitch of trailing vortex wake (x/r_0=0.65)

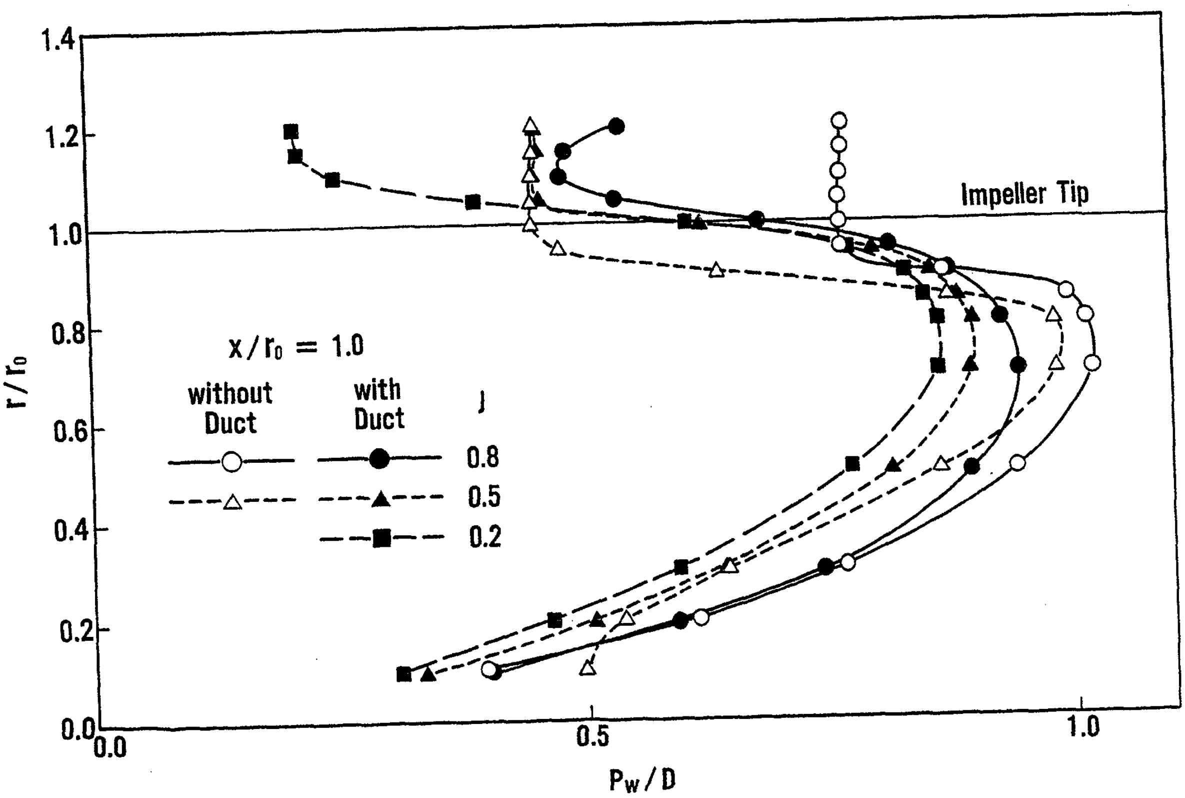

Fig. 12 Comparison of hydrodynamic pitch of trailing vortex wake (x/r_0=1.00)

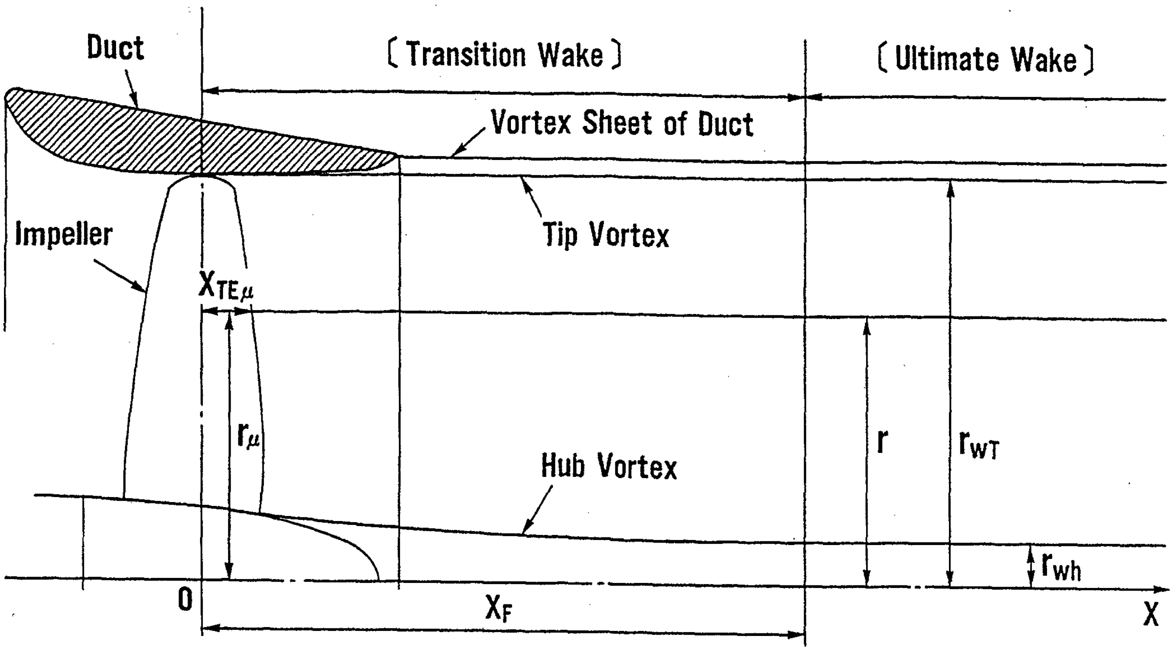

Fig. 13 Model of trailing vortex wake of ducted propeller

where,

$$\alpha_\mu=\begin{cases}0 & \text{for} \quad \mu=1,\\ \dfrac{(2\mu-1)\pi}{2(N_R+1)} & \text{for} \quad \mu=2,3,\cdots,N_R+1.\end{cases}$$

Radial positions of trailing vortex sheet at the trailing edge of the impeller blade must coincide with those of the panel strips on the blade surface expressed as

$$r_\mu=\frac{1}{2}(r_0+r_h)-\frac{1}{2}(r_0-r_h)\cos\alpha_\mu, \tag{3.2}$$

where r_h is the hub radius. Then variations of the radial positions of trailing vortex panel strips in the transition wake region can be approximated by a polynomial expression as

$$r_{t\mu}=r_\mu-(r_\mu-r_{w\mu})\cdot f_r(\xi), \tag{3.3}$$

where,

$$f_r(\xi)=\sqrt{\xi}+1.013\xi-1.920\xi^2 +1.228\xi^3-0.321\xi^4, \tag{3.4}$$

$$\xi=\frac{x-x_{TE}}{x_F-x_{TE}},$$

x_{TE}=x-coordinate at trailing edge of blade,

x_F=x-coordinate of the point where the ultimate wake region starts.

$f_r(\xi)$ is the same expression for the conventional propeller by Hoshino[2].

On the basis of the measured results, the radius of the tip vortices in the ultimate wake region can be expressed as a function of slip ratio as follows:

$$r_{wT}/r_0=\begin{cases}1.0 & \text{for ducted propeller,}\\ 0.929-0.162s & \text{for impeller without duct,}\end{cases} \tag{3.5}$$

where,

s=slip ratio$=1-J/p$,

p=pitch ratio at 0.7 radius.

The radius of the hub vortex and axial coordinate of the starting point of the ultimate wake are kept constant as

$$r_{wh}/r_0=0.1, \quad x_F/r_0=2.0. \tag{3.6}$$

The variation of the radial positions of the center of the tip vortices calculated by the above equations are shown in Fig. 14, comparing with those obtained from the results of the flow measurements by LDV. In this formula, as the contraction of the trailing vortex wake of the ducted propeller is found to be fairly small, the contraction is ignored.

Secondly the variation of the hydrodynamic pitch is considered. The hydrodynamic pitch of the helical trailing vortex sheet which flows from the radial position r_μ is constant in the ultimate wake region as follows:

$$P_{u\mu}=P_{w\mu}\cdot f_P(\eta), \tag{3.7}$$

where,

$$P_{w\mu}/P_{G\mu}=\begin{cases}0.993-0.251s & \text{for ducted propeller,}\\ 0.874+0.067s & \text{for impeller without duct,}\end{cases}$$

$$f_P(\eta)=\begin{cases}0.594+1.076\eta-0.852\eta^2+1.351\eta^3-1.411\eta^4 & \text{for ducted propeller,}\\ 0.579+0.387\eta+1.073\eta^2+0.393\eta^3-1.435\eta^4 & \text{for impeller without duct,}\end{cases} \tag{3.8}$$

$$\eta=\frac{r_{w\mu}-r_{wh}}{r_{wT}-r_{wh}},$$

$P_{G\mu}$=geometrical pitch at radial position r_μ.

The above polynomial expressions of $P_{w\mu}/P_{G\mu}$ and $f_P(\eta)$ based on $\eta=0.5$ approximate the measurement data, and are shown in Fig. 15. The hydrodynamic pitch $P_{w\mu}$ in the ultimate wake region of the ducted propeller decreases at the slip ratio increases while the opposite is the case for the impeller without duct. The

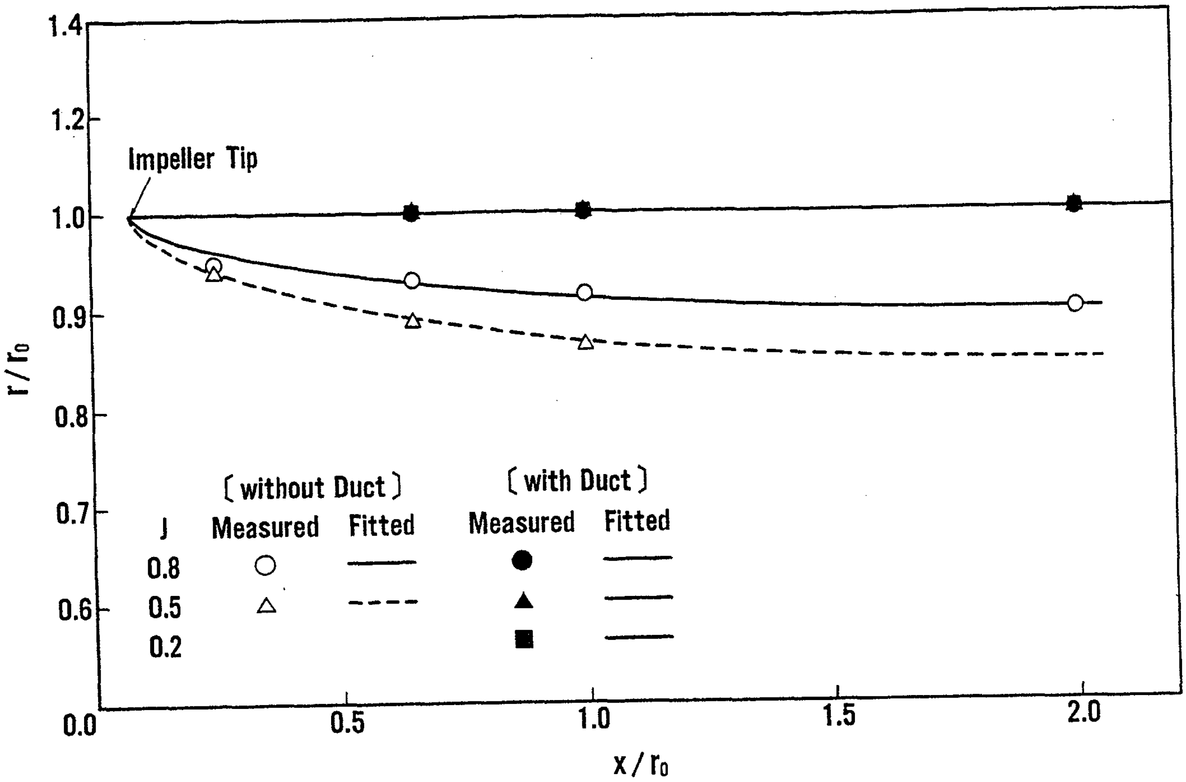

Fig. 14 Comparison of contraction of trailing vortex wake

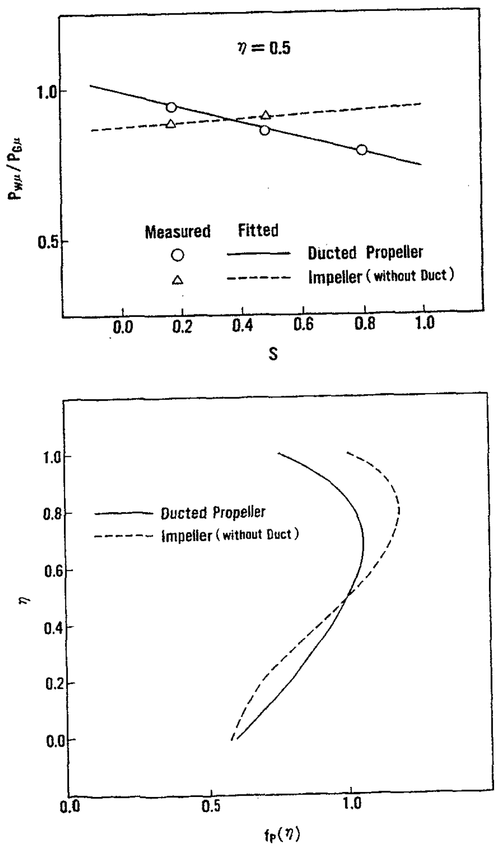

Fig. 15 Comparison of modeled hydrodynamic pitch

hydrodynamic pitch of trailing vortex sheet in the transition wake region changes smoothly from the geometrical pitch $P_{G\mu}$ to the hydrodynamic pitch $P_{u\mu}$ in the ultimate wake region. The variation of the hydrodynamic pitch $P_{t\mu}$ in the transition wake region can be approximated by a polynomial expression as

$$P_{t\mu}=[P_{G\mu}-(P_{G\mu}-P_{w\mu})\cdot f_r(\xi)]f_P(\eta). \qquad (3.9)$$

Nextly, let us consider more theoretical wake model. In the case of ducted propellers, it may be practical to construct the wake model by the use of the thrust ratio τ as a parameter instead of the slip ratio s in order to predict the performance for several ducted propellers. τ is defined as

$$\tau=T_P/T, \qquad (3.10)$$

where T_P is impeller thrust and T is total thrust. Then, the relation between the contraction, the hydrodynamic pitch of the ducted propeller and the thrust ratio based on the open-water test results is considered as follows:

The ratio of the ducted propeller wake radius r_∞ at the infinite downstream to the impeller radius r_0 can be obtained by the momentum theory[6] as shown in Fig. 16, comparing with the measured data. The tip vortex radius r_{wT} in the ultimate wake region is almost equal to the value obtained by the momentum theory in the range of the thrust ratio from 0.5 to 0.8. The operating condition of the ducted propeller is mostly in this range. Therefore, the contraction of the trailing vortex wake of the ducted propeller is obtained by the momentum theory instead of Eq. (3.5).

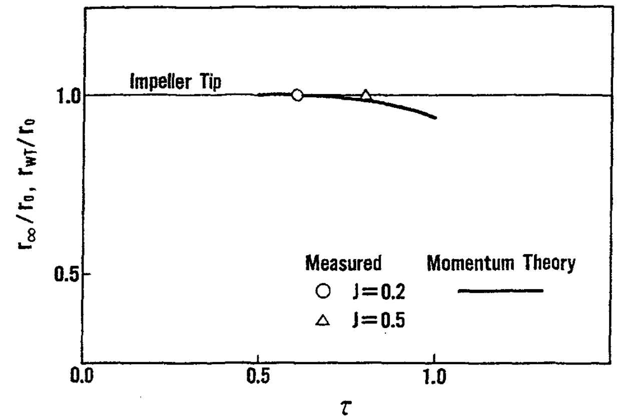

Fig. 16 Comparison of radius of trailing vortex wake

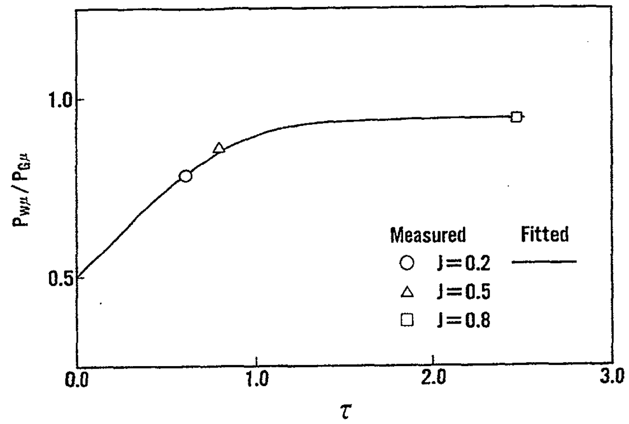

Fig. 17 Hydrodynamic pitch based on thrust ratio

Instead of Eq. (3.8), the hydrodynamic pitch $P_{w\mu}$ in the ultimate wake region of the ducted propeller based on the thrust ratio can be approximated by a polynomial expression as

$$P_{w\mu}/P_{G\mu}=0.5+0.420\tau+0.402\tau^2-0.701\tau^3+0.323\tau^4-0.049\tau^5, \tag{3.11}$$

and are shown in Fig. 17, together with the measured data.

In the present calculation based on the thrust ratio, the thrust ratio is determined by the iterative procedure. The first solution is obtained by the use of the wake model based on the slip ratio. The iterations are continued until convergence on the thrust ratio is achieved.

In this paper, two kinds of wake models are called Wake S and Wake τ. Wake S is based on the slip ratio and Wake τ is based on the thrust ratio.

3.2 Formulation of Field Point Velocity

The induced velocity at field point P outside the boundary surface S, which is composed of impeller blade surface S_B, hub surface S_H, duct surface S_D, impeller wake surface S_{WB} and duct wake surface S_{WD}, can be evaluated by taking the gradient of the velocity potential ϕ. Using the relative inflow velocity $\boldsymbol{V}_I$ and the unit outward normal vector $\boldsymbol{n}_Q$ to the surface S, the field point velocity can be expressed as

$$\begin{aligned}\boldsymbol{v}(P)&=\nabla_P\phi(P)\\&=\frac{1}{4\pi}\iint_{S_B+S_H+S_D}\phi(Q)\nabla_P\frac{\partial}{\partial n_Q}\left(\frac{1}{R(P,Q)}\right)dS\\&\quad+\frac{1}{4\pi}\iint_{S_{WB}+S_{WD}}\Delta\phi(Q')\nabla_P\frac{\partial}{\partial n_{Q'}}\left(\frac{1}{R(P,Q')}\right)dS\\&\quad+\frac{1}{4\pi}\iint_{S_B+S_H+S_D}(\boldsymbol{V}_I\cdot\boldsymbol{n}_Q)\nabla_P\left(\frac{1}{R(P,Q)}\right)dS\end{aligned} \tag{3.12}$$

where $R(P, Q)$ is the distance from the field point P to the boundary point Q and $\partial/\partial n_Q$ is the normal derivative to the boundary surface S.

Here, the blade, hub and duct surfaces are divided into N small panels S_j. Thus, the impeller and the duct are divided into N_P and N_D small panels respectively. The duct wake surface between adjacent two blades is divided into N_L wake strips. And each wake strip is divided into L wake panels. Then, the wake surfaces of the impeller and the duct are divided into $(N_R\times L)$ and $(N_L\times L)$ small panels respectively. The potential ϕ, the potential jump $\Delta\phi$ and the normal component of velocity $(\boldsymbol{V}_I\cdot\boldsymbol{n}_Q)$ are assumed to be constant within each panel and equal to the values ϕ_j, $\Delta\phi_j$, $(\boldsymbol{V}_I\cdot\boldsymbol{n}_j)$ at the centroid of each panel, respectively. Eq. (3.12) can be approximated by

$$\boldsymbol{v}_i=\sum_{j=1}^{N}\phi_j\nabla_P C_{ij}+\sum_{j=1}^{N_l}\Delta\phi_j\nabla_P W_{ij}-\sum_{j=1}^{N}(\boldsymbol{V}_I\cdot\boldsymbol{n}_j)\nabla_P B_{ij}, \tag{3.13}$$

for $i=1, 2, \cdots, N$, $N=N_P+N_D$, $N_l=N_R+N_L$.

Here, $\nabla_P C_{ij}$, $\nabla_P B_{ij}$ and $\nabla_P W_{ij}$ are the influence coefficients defined by

$$\begin{aligned}\nabla_P C_{ij}&=\sum_{k=1}^{K}\left[\frac{1}{4\pi}\iint_{S_j}\nabla_P\frac{\partial}{\partial n_j}\left(\frac{1}{R_{ijk}}\right)dS_j\right],\\\nabla_P W_{ij}&=\sum_{k=1}^{K}\sum_{l=1}^{L}\left[\frac{1}{4\pi}\iint_{S_l}\nabla_P\frac{\partial}{\partial n_l}\left(\frac{1}{R_{ilk}}\right)dS_l\right],\\\nabla_P B_{ij}&=\sum_{k=1}^{K}\left[-\frac{1}{4\pi}\iint_{S_j}\nabla_P\left(\frac{1}{R_{ijk}}\right)dS_j\right].\end{aligned} \tag{3.14}$$

where,

K=number of impeller blades.

If the surface element of the ducted propeller are approximated by a number of quadrilateral hyperboloidal panels, the influence coefficients are evaluated analytically in near field. On the other hand, they are approximated by a Taylor series expansion in the far field in order to save computation time.

4. Comparison with Experimental Data

4.1 Open-Water Characteristics

The open-water characteristics of both the ducted propeller and the impeller without duct which were used in the flow field measurement were calculated by the present panel method with the new wake model. The panel arrangements of the ducted propeller are shown in Fig. 18. The panel arrangements of trailing vortex wake of the ducted propeller at the advance ratio of $J=0.50$ are illustrated in Fig. 19, comparing with those of the impeller without duct. It is clearly shown that the deformation of the trailing vortex wake of the ducted

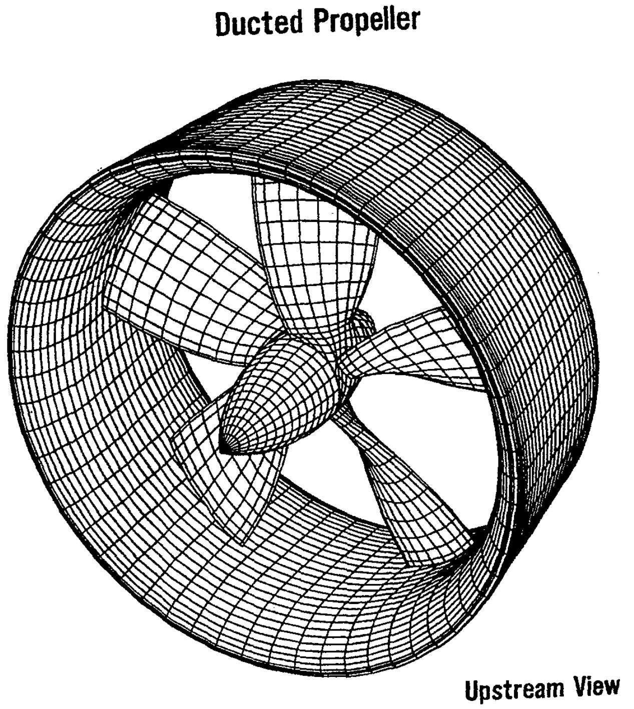

Fig. 18 Panel arrangement for ducted propeller used in flow measurements

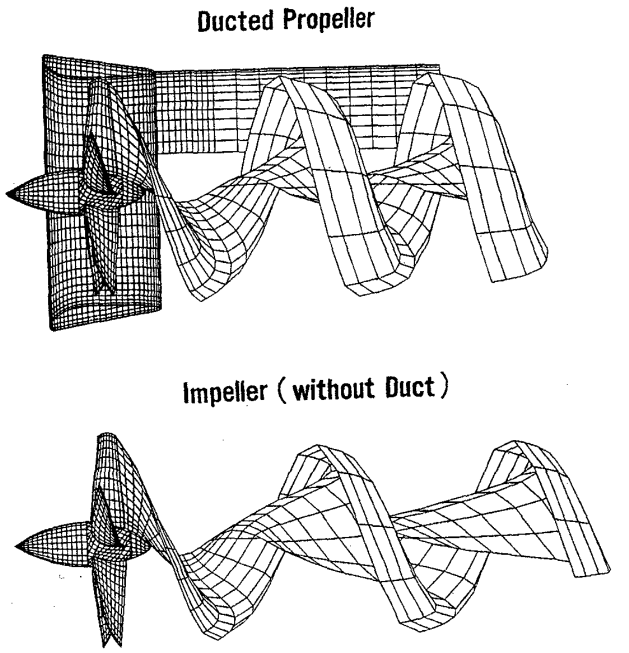

Fig. 19 Comparison of new wake models between ducted propeller and impeller without duct

propeller is smaller than that of the impeller without duct for the effect of small contraction.

Here, the impeller thrust T_P, duct thrust T_D and total thrust T and torque Q of the ducted propeller can be expressed in the nondimensional forms which are the thrust coefficient K_T, torque coefficient K_Q, impeller thrust coefficient K_{TP} and duct thrust coefficient K_{TD} as follows:

$$K_T=\frac{T}{\rho n^2 D^4}=\frac{T_P+T_D}{\rho n^2 D^4},\quad K_Q=\frac{Q}{\rho n^2 D^5},$$
$$K_{TP}=\frac{T_P}{\rho n^2 D^4},\quad K_{TD}=\frac{T_D}{\rho n^2 D^4},\tag{4.1}$$

where,

ρ=density of water.

The calculated results of the impeller without duct are shown in Fig. 20, comparing with the experimental data. The thrust coefficient K_T and the torque coefficient K_Q are in good agreement with experimental data. On the other hand, the comparison between the calculations and experiments of the ducted propeller are shown in Fig. 21. The impeller thrust coefficient K_{TP} and the

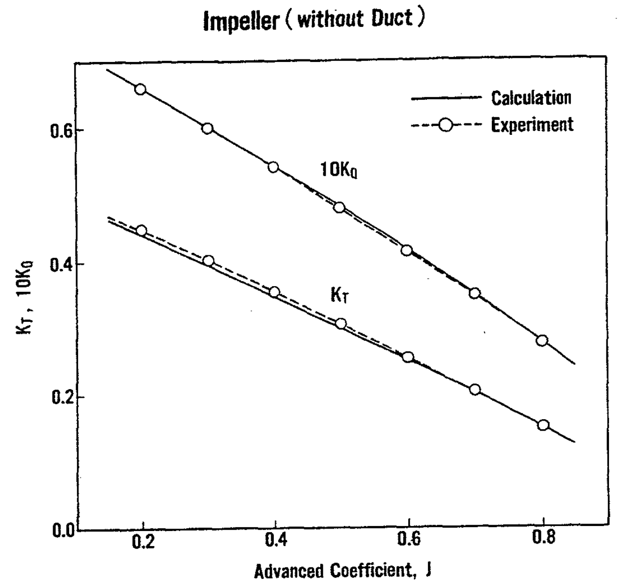

Fig. 20 Comparison of open-water characteristics for impeller without duct

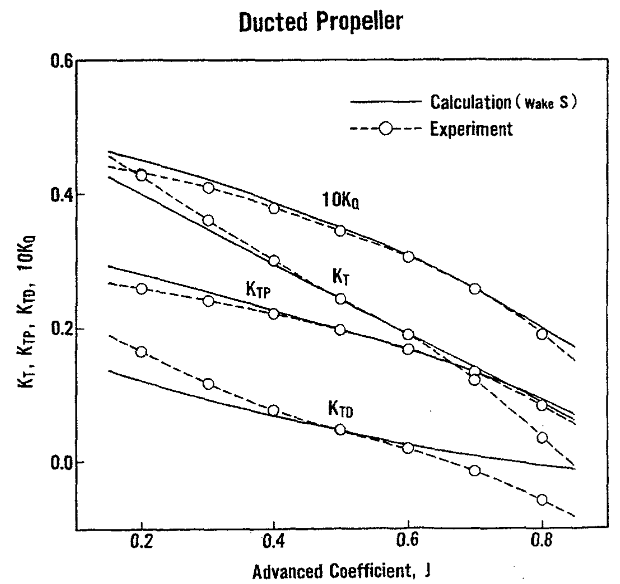

Fig. 21 Comparison of open-water characteristics for ducted propeller

torque coefficient K_Q are in good agreement with experimental data over a wide advance ratio. But the duct thrust coefficient K_{TD} is larger at low advance ratio and smaller at high advance ratio than experimental data. This discrepancy may be partially due to neglect of the flow separation from the duct.

4.2 Velocity at Field Point

In order to evaluate the accuracy of the present method, flow field around the ducted propeller were calculated and compared with the measurements by LDV. Comparison of the velocity distribution of the ducted propeller at axial position of $x/r_0=1.00$ and at the advance ratio of $J=0.50$ is shown in Fig. 22 in the form of equi-velocity contour curves and shown in Fig. 23 as the velocity vectors in a plane parallel to the propeller plane. The calculated result of the axial velocity v_x generally agrees with the experimental one though it is slightly smaller in the vicinity of the radial position $r/r_0=0.70$.

Radial distributions of the circumferentially averaged

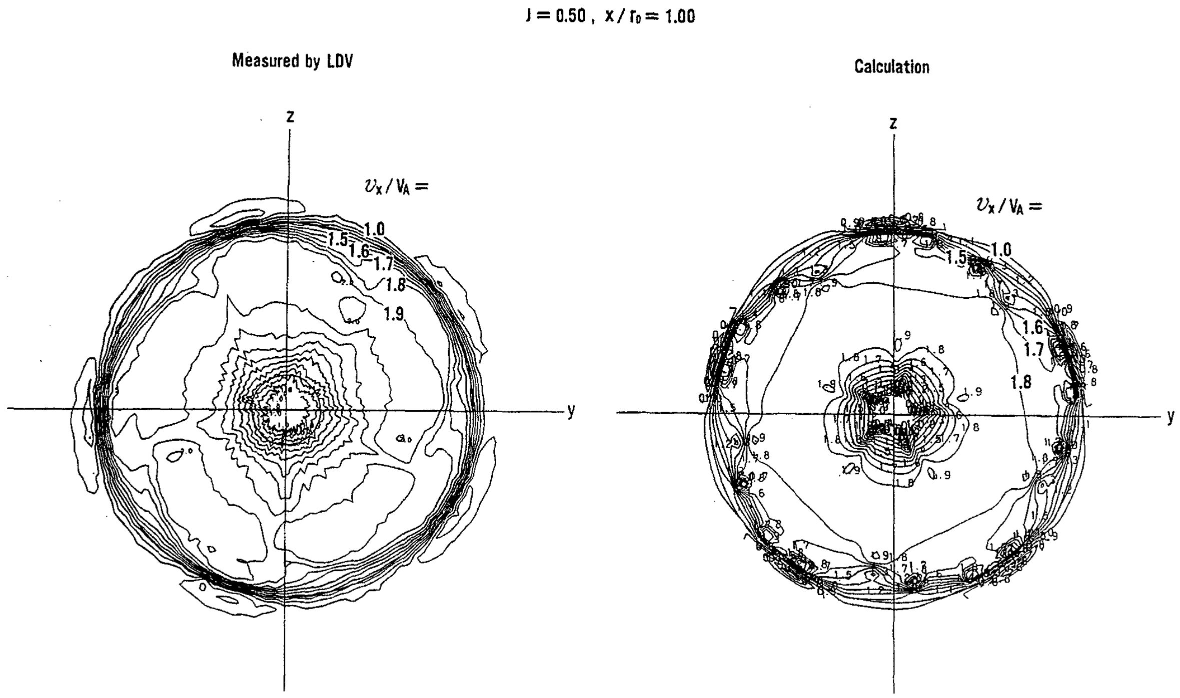

Fig. 22 Comparison of axial components of velocities downstream of ducted propeller ($J=0.50$, $x/r_0=0.65$)

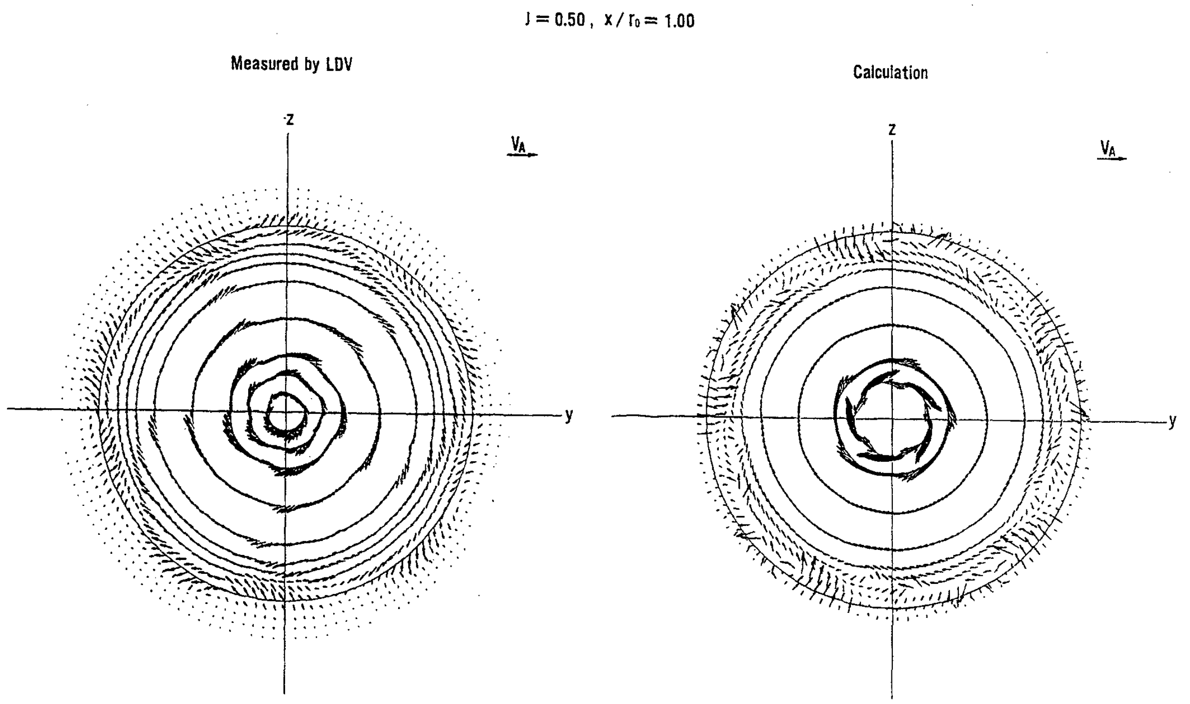

Fig. 23 Comparison of cross components of velocities downstream of ducted propeller ($J=0.50$, $x/r_0=0.65$)

velocities calculated by the present method are compared with the measurements as shown in Fig. 24. The agreement between the calculations and the measurements is generally good. However, there are disagreements in the tangential velocities at the small radial positions. This discrepancy may be improved by considering a hub vortex in our wake model. The radial velocities are nearly equal to zero. This phenomenon may cause the small contraction of the trailing vortex wake of the ducted propeller.

5. Numerical Applications

5.1 NSMB Ka4-55 in nozzle no. 19

In order to evaluate the applicability of the present wake model for ducted propellers, comparative calculations were conducted for ducted propellers with published experimental open-water characteristics. Firstly, NSMB (now MARIN) Ka4-55 screw in nozzle no. 19 was selected[7]. This ducted propeller illustrated in Fig. 25 has four blades with an expanded area ratio of 0.55 and pitch ratio at 0.7 radius of 1.0. The open-water characteristics calculated by the present method with two kinds of wake models which are based on the slip ratio s and the thrust ratio τ are shown in Fig. 26, comparing with the experiments and the calculation by van Houten[8] using a lifting surface theory. The calculated results by the present method are in better agreement with the experimental data over a wide range of advance ratio than the calculated results by van Houten. The duct thrust coefficient K_{TD} is larger at low advance ratio and smaller at high advance ratio than experimental data. This tendency is the same as the ducted propeller used in flow measurements. The results with τ based wake model is slightly close to the experi-

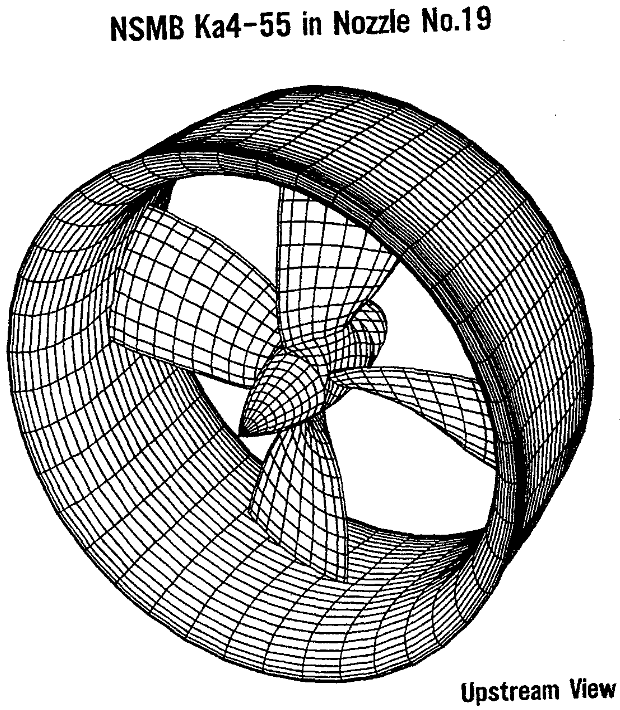

Fig. 25 Panel arrangement for NSMB Ka4-55 in nozzle no. 19

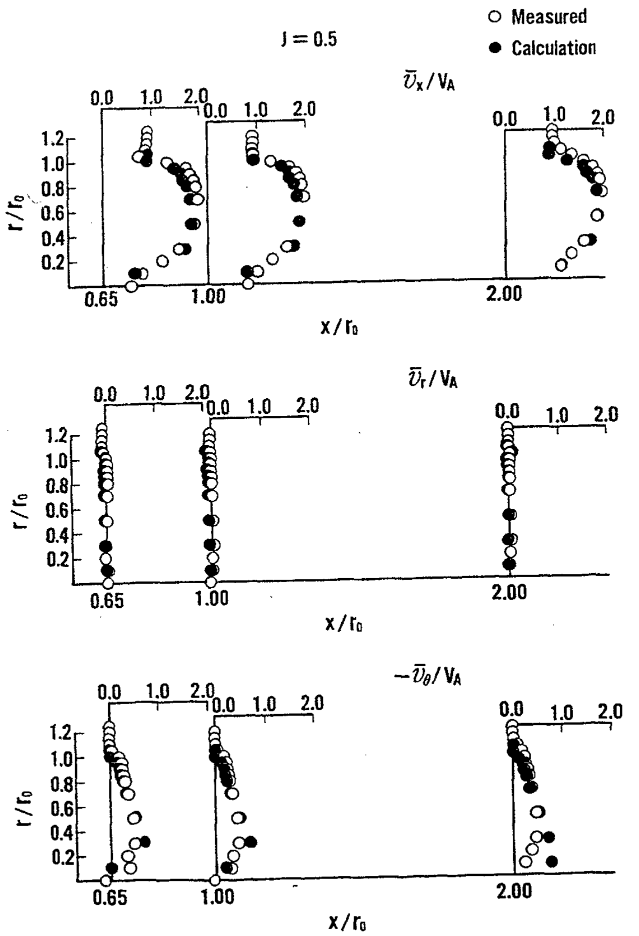

Fig. 24 Comparison of circumferentially averaged velocities for ducted propeller

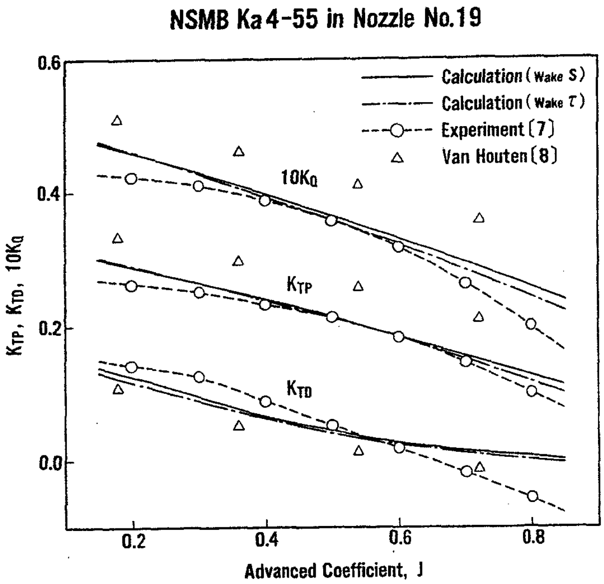

Fig. 26 Comparison of open-water characteristics for NSMB Ka4-55 in nozzle no. 19

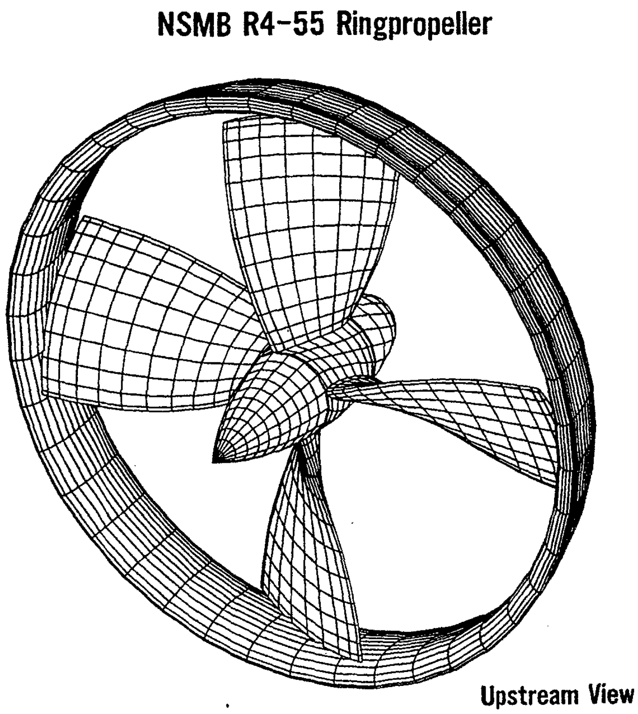

Fig. 27 Panel arrangement for NSMB R4-55 ringpropeller

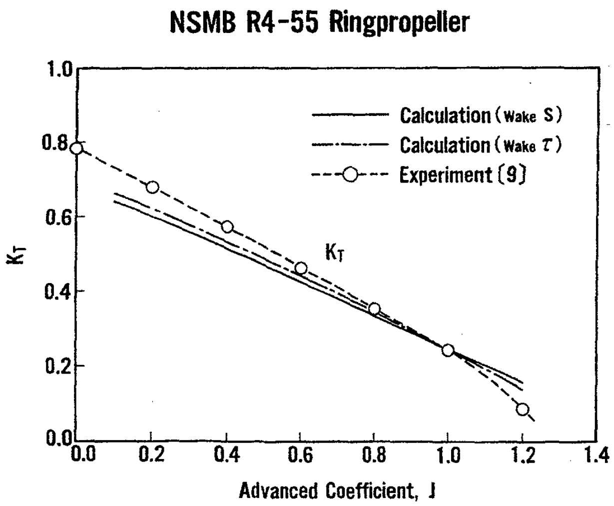

Fig. 28 Comparison of open-water characteristics for NSMB R4-55 ringpropeller

mental data.

5.2 NSMB R4-55 ringpropeller

Next application was made for NSMB R4-55 ringpropeller[9] as an example of extremely different duct length-impeller diameter ratio. A ringpropeller is a kind of a ducted propeller but the impeller blade tips attach to the ring which rotates with the impeller. This ring propeller illustrated in Fig. 27 has four blades with an expanded area ratio of 0.55, pitch ratio at 0.7 radius of 1.4 and duct length-impeller diameter ratio of 0.15. The open-water characteristics calculated by the present method with two kinds of wake models are shown in Fig. 28. The calculated results are in good agreement with the experimental data, and the results with the thrust ratio based wake model are in better agreement with the experimental data than the results with the slip ratio based wake model.

6. Concluding Remarks

The flow field downstream of a ducted propeller and a impeller without duct were investigated precisely by the use of a 3-component LDV. Comparison of velocity measurements clearly shows the effect of duct. Based on the measured velocity distributions downstream of the ducted propeller, new wake models of the trailing vortex wake based on both the slip ratio and the thrust ratio were proposed. Calculations by the present method and the measurements led to the following conclusions:

(1) The strength of the tip vortices of the impeller of the ducted propeller becomes weaker than that of the impeller without duct due to the effect of duct.

(2) The contraction of the trailing vortex wake of the ducted propeller is fairly small in the range of the thrust ratio τ from 0.5 to 0.8 which is in the usual operating condition of the ducted propeller.

(3) The hydrodynamic pitch of the ducted propeller in the vicinity of the radial position $r/r_0=0.70$ becomes smaller than that of the impeller without duct due to small contraction.

(4) Flow field around a ducted propeller can be predicted fairly well by the present panel method.

(5) Open-water characteristics of ducted propellers calculated by the present method are also in good agreement with experimental ones.

(6) The iteration method with the experimental wake model based on the thrust ratio can predict more precisely than the method based on the slip ratio.

Acknowledgements

The author would like to express his sincere gratitude to Dr. Kayo, Manager of the Ship and Ocean Engineering Laboratory of the Nagasaki Research and Development Center, Mitsubishi Heavy Industries, Ltd., and Mr. N. Chiba and Dr. T. Hoshino of the same laboratory for their guidance and encouraging discussions. Thanks are also extended to all the members of the Nagasaki Experimental Tank for their cooperation.

Reference

1) Kawakita, C.: Hydrodynamic Analysis of a Ducted Propeller in Steady Flow Using a Surface Panel Method, The West-Japan Society of Naval Architects, No. 84, (Aug. 1992).

2) Hoshino, T.: Hydrodynamic Analysis of Propellers in Steady Flow Using a Surface Panel Method, 2nd Report: Flow Field around Propeller, Journal of the Society of Naval Architects of Japan, Vol. 166, (Dec. 1989), pp. 79-92.

3) Falcão de Campos, J. A. C. : On the calculation of Ducted Propeller Performance in Axisymmetric Flows, Technical Report 696, NSMB, Wageningen, the Netherlands, (1983).
4) Kinnas, S. A., Hughes, M. J., and Kerwin, J. E. : Comparison of Analysis and Experiment for a Ducted Propeller, In Proceedings of the 2nd International Symposium on Performance Enhancement for Marine Applications, Newport, Rhode Island, (Oct. 1990), pp. 153-164.
5) Hoshino, T. and Oshima, A. : Measurement of Flow Field around Propeller by Using a 3-Component Laser Doppler Velocimeter (LDV), Mitsubishi Technical Review, Vol. 24, No. 1, (Feb. 1978), pp. 46-53.
6) Kato, H. : Introductory Remarks on Marine Propellers, The Third Symposium on Marine Propellers, The Society of Naval Architects of Japan, (Jul. 1987), pp. 1-22.
7) van Manen, J. D. : Effect of Radial Load Distribution on the Performance of Shrouded Propellers, Trans. RINA, Vol. 105, (1963), pp. 59-74.
8) van Houten, R. : Analysis of Ducted Propellers in Steady Flow, Technical Reprot 4. 76-1, Airflow Research and Manufacturing Corp., Watertown, MA., (Feb. 1986).
9) van Gunsteren, L. A. : Ring Propellers and Their Combination with a Stator, Marine Technology, Vol. 7, No. 4, (Oct. 1970), pp. 433-448.